Ultrahigh-Power-Factor Carbon Nanotubes and an Ingenious Strategy for Thermoelectric Performance Evaluation

Wenbin Zhou, Qingxia Fan, Qiang Zhang, Kewei Li, Le Cai, Xiaogang Gu, Feng Yang, Nan Zhang, Zhuojian Xiao, Huiliang Chen, Shiqi Xiao, Yanchun Wang, Huaping Liu, Weiya Zhou, and Sishen Xie**

Owing to outstanding electrical properties and unique advantages compared with the traditional inorganic semiconductor, the carbon nanotube (CNT) based films have attracted considerable attentions in flexible thermoelectric (TE) applications.[1–12] The TE performance can be evaluated by the figure-of-merit, $ZT = S^2\sigma T/\kappa$, where S, σ, κ, and T are the Seebeck coefficient, electrical conductivity, thermal conductivity, and absolute temperature, respectively. $PF = S^2\sigma$ is defined as thermoelectric power factor, which is directly related to the usable power attainable from the TE materials.[7]

However, almost all the previous researches focused on the CNT-based films prepared from the dispersed CNT solutions, which exhibit relatively low power factors.[7–11] On the other hand, the measurement of in-plane thermal conductivity for the CNT-based film is full of challenges, especially for thin films (thickness < 1 μm), which impedes evaluation and improvement of TE performance. Instead, previous researchers estimated the TE performance by measuring out-of-plane thermal conductivity or citing literature values of other similar CNT specimens (Table S1, Supporting Information), while the power factor was measured in the in-plane direction.[3,8,10–12]

Typical measuring techniques of thermal conductivity, such as the steady heat flow method, laser flash method,[3,11] etc., require large size specimens and cannot obtain in-plane thermal conductivity of films. The 3ω-method can be used to investigate the in-plane thermal conductivity of films,[13–15] while this method requires complicated measuring system and suffers from weak signal-to-noise ratio, in addition, patterned metal detectors and thin SiN_x insulated layer need to be deposited on the surface of conductive films.[13,14] Recently, researchers have carried out the measurement of in-plane thermal conductivity for thick CNT buckypaper by a self-heating method, in which non-contact infrared thermometer was used to measure temperature distribution of the heated films.[16–18] Itkis et al. measured thermal conductivity of single-walled carbon nanotube (SWNT) thin films by a bolometric technique, where infrared radiation was used as a heat source and the influence of blackbody radiation was limited by a quartz filter.[19] However, it is inconvenient to introduce relatively complicated optical system in the high vacuum chamber. Particularly, for very thin CNT films, heat losses through convection and radiation are noteworthy because of the large surface area to volume ratio and approximate blackbody emissivity. Therefore, it possibly causes some deviation if the heat losses are not accurately taken into account during the measurement.

Here, we have first found the as-grown SWNT interconnected films and SWNT fibers obtained by twisting these films possess enormous potential of thermoelectric applications because of their ultrahigh power factors, PF_{max} = 2482 μW m^{-1} K^{-2} at room temperature. It is among the highest value ever reported for flexible TE materials and approximately half of the state-of-the-art inorganic TE materials (Bi_2Te_3).[8–12,14,20–23] Furthermore, these SWNT-based materials avoid tedious composite technology and have low density (≈1 g cm^{-3}) in comparison to that of Bi_2Te_3 (≈7.86 g cm^{-3}).[1] These SWNT films can be directly synthesized

Prof. W. B. Zhou, Q. X. Fan, Q. Zhang, K. W. Li, Dr. L. Cai,[+] X. G. Gu, F. Yang, N. Zhang, Z. J. Xiao, H. L. Chen, S. Q. Xiao, Dr. Y. C. Wang, Prof. H. P. Liu, W. Y. Zhou, Prof. S. S. Xie
Beijing National Laboratory for Condensed Matter Physics
Institute of Physics
Chinese Academy of Sciences
Beijing 100190, China
E-mail: wyzhou@aphy.iphy.ac.cn; ssxie@aphy.iphy.ac.cn

Prof. W. B. Zhou, Q. X. Fan, Q. Zhang, K. W. Li, Dr. L. Cai, X. G. Gu, F. Yang, N. Zhang, Z. J. Xiao, H. L. Chen, S. Q. Xiao, Dr. Y. C. Wang, Prof. H. P. Liu, W. Y. Zhou, Prof. S. S. Xie
Beijing Key Laboratory for Advanced Functional Materials and Structure Research
Beijing 100190, China

Prof. W. B. Zhou, Q. X. Fan, Q. Zhang, K. W. Li, Dr. L. Cai, X. G. Gu, F. Yang, N. Zhang, Z. J. Xiao, H. L. Chen, S. Q. Xiao, Dr. Y. C. Wang, Prof. H. P. Liu, W. Y. Zhou, Prof. S. S. Xie
University of Chinese Academy of Sciences
Beijing 100190, China

[+]Present address: Department of Electrical and Computer Engineering, Michigan State University, East Lansing, MI 48824, USA

DOI: 10.1002/smll.201600501

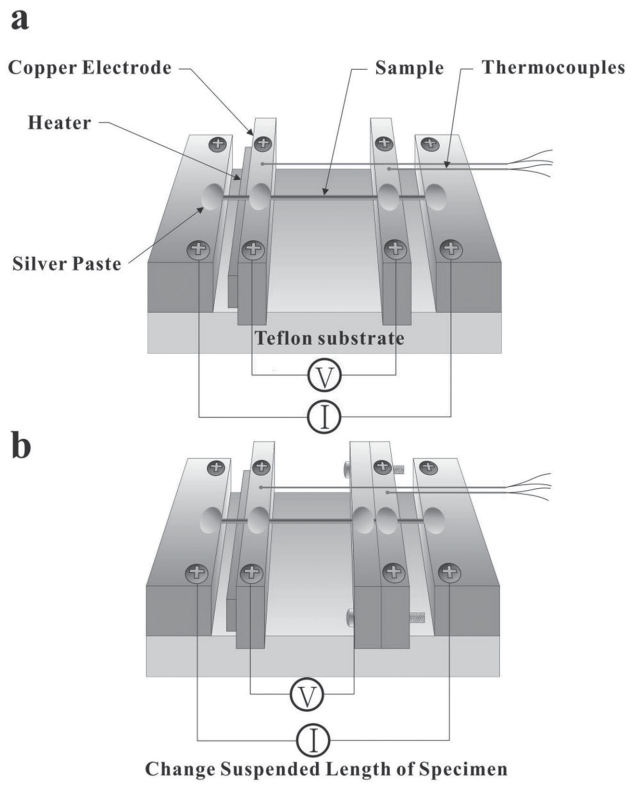

Figure 1. Schematic illustration for measuring thermoelectric properties of films or fibers. A schematic of specimen stage configuration with a) an initial and b) changed suspended length of a specimen.

by floating catalyst chemical vapor deposition reported in our previous researches.[24,25] The continuous conductive network of CNT was formed when they are growing at high temperature, which resulting in more superior structure and electrical properties. What is more, we provide an ingenious strategy for accurately evaluating the thermoelectric performance of CNT films in the in-plane direction and fibers in the axial direction, where thermoelectric properties (thermal conductivity, electrical conductivity, and Seebeck coefficient) in the same direction can be measured efficiently for the same specimen. For the CNT thin film, the huge influence of the heat losses through convection and radiation are eliminated during the measurement of in-plane thermal conductivity. Our measurement method and apparatus were verified by measuring various standard film and fiber specimens, all the results coincided with the reference values and the deviations were negligible (Table S2, Supporting Information). As a consequence, we can take advantage of our measuring method and apparatus to systematically investigate the thermoelectric properties of the as-prepared SWNT films and fibers.

The schematic illustration of our approach and apparatus for thermoelectric properties measurements is shown in **Figure 1**. We design a specific testing stage (Figure 1a), four copper electrodes are fixed on the insulated Teflon substrate. A film ribbon or fiber is suspended across the copper electrodes and pasted by high-purity silver paste to form perfect electrical and thermal contacts. The copper electrodes can act as heat sinks because of their high thermal conductivity and heat capacity. Thus, two ends of specimen always maintain the ambient temperature (T_0) during the measurement of thermal conductivity. The length (L) of the suspended specimen between the two inside electrodes can be changed by inserting thin copper electrodes. As shown in Figure 1b, we can insert carefully a thin copper electrode between the two inside electrodes and make it to contact closely with one of inside electrodes by screws. Additional high-purity silver paste is added on the contact region between sample and thin copper electrode. Consequently, the suspended length of the same sample was decreased. A heater and two T-type thermocouples are fixed on the two inside copper electrodes with intimate contacts. Before the measurement, the stage is placed in a temperature-controlled chamber.

Figure 2a shows the optical photograph of a rectangular piece cut from a homogeneous as-grown SWNT film. The film was cut into a 30 mm × 0.75 mm ribbon and densified with ethanol, which has a thickness of 316 ± 14 nm. The densified ribbon was suspended across the copper electrodes with a suspended length of 16 mm. After long time vacuum pumping, the temperature-controlled testing chamber reached a stabilized vacuum of 6×10^{-4} Pa. The measurement of thermal conductivity in our work is based on the 1D heat transfer equation. When the suspended film ribbon or fiber is heated by a constant direct current (I), a uniform heat flux will spread along the specimen. In a high vacuum of 10^{-4} Pa, the heat loss through convection can be eliminated (Figure S1, Supporting Information). Taking the heat loss through radiation into account, we can write the heat transfer equation in steady state as

$$\kappa \frac{\mathrm{d}^2T(x)}{\mathrm{d}x^2} + \frac{I^2R - P_{\mathrm{rad}}}{LA_{\mathrm{sec}}} = 0 \tag{1}$$

where R and A_{sec} represent the resistance under heating current and the cross section area of the suspended specimen. P_{rad} is the power of radiant heat loss. The average temperature increment ΔT ($\Delta T = T - T_0$, T is the average temperature of the heated suspended specimen) is restricted in the range of 2–6 K by adjusting the current value, so P_{rad} can be expressed as $P_{\mathrm{rad}} \approx 4\varepsilon\sigma A_{\mathrm{rad}} T_0^3 \Delta T$ (Figure S2, Supporting Information), where $\sigma = 5.67 \times 10^{-8}$ W m^{-2} K^{-4}, ε, and A_{rad} are Stefan–Boltzmann constant, emissivity, and radiant area of the specimen, respectively. For bulk specimens, the radiant area A_{rad} is the surface area A. We defined $g_{\mathrm{rad}} = \frac{4\varepsilon\sigma A_{\mathrm{rad}} T_0^3}{LA_{\mathrm{sec}}}$ as the radiant heat loss coefficient.

Additionally, it will exhibit a linear $R - T$ relationship ($R = a + bT$) when the temperature of the specimen varies in a small range. Based on theoretical analysis above, we can obtain the solution (see the Supporting Information for experimental details) of Equation (1)

$$\frac{1}{R} = \frac{1}{R_0} - \frac{L}{(12\kappa + g_{\mathrm{rad}}L^2)A_{\mathrm{sec}}} b \frac{1}{R_0} I^2 \tag{2}$$

which indicates that the reciprocal of resistance varies linearly with the square of the current. So we can increase heating current gradually to measure a series of resistances for fitting $R^{-1} - I^2$ curve. Then the expression of thermal conductivity κ can be obtained from the slope k of $R^{-1} - I^2$ curve

DOI: 10.1002/smll.201600501

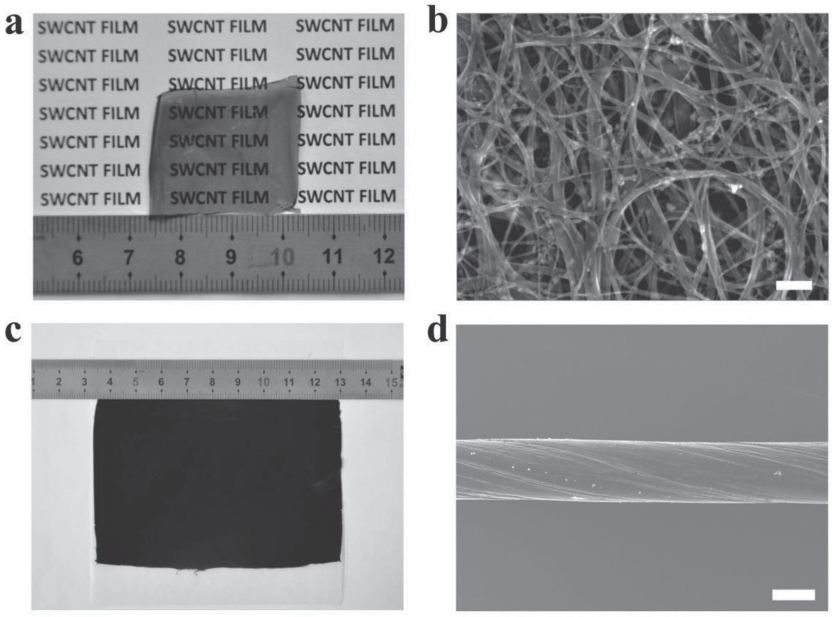

Figure 2. Morphology characterization of the CNT specimens. a) The optical photograph and b) the SEM image of a rectangular piece cut from a homogeneous as-grown SWNT film (scale bar, 100 nm). c) The optical photograph of a CNT sheet, which was composed of multilayer continuously synthesized CNT films and densified by ethanol. d) The SEM image of a SWNT fiber with a diameter of 29 μm (scale bar, 20 μm), which was obtained by twisting a 40 mm × 5 mm SWNT ribbon.

$$\kappa = -\frac{L}{12A_{\text{sec}}}\frac{1}{R_0}\frac{b}{k} - \frac{g_{\text{rad}}L^2}{12} \quad (3)$$

where R_0 is the resistance of the suspended specimen under T_0, R_0^{-1} can be obtained directly from the intercept of $R^{-1} - I^2$ curve. We defined $\kappa_{\text{ap}} = -\frac{L}{12A_{\text{sec}}}\frac{1}{R_0}\frac{b}{k}$ as the apparent thermal conductivity without a consideration of the radiant heat loss and Equation (3) can be expressed by $\kappa_{\text{ap}} = \kappa + \frac{g_{\text{rad}}L^2}{12}$, which indicates a linear relationship between the apparent thermal conductivity and the square of the suspended length. If the radiant power is minor compared with the heating power, the radiant heat loss can be neglected, such as a platinum fiber (Figure S3, Supporting Information), then $\kappa \approx \kappa_{\text{ap}}$. But for SWNT thin films, the radiant heat loss is noteworthy because of the large surface area to volume ratios and approximate blackbody emissivity ($\varepsilon \approx 1$). Consequently, we should eliminate the influence of radiant heat loss during the measurement.

We measured the resistances of the suspended SWNT ribbon under different current causing observable heating effects. **Figure 3**a shows the resistance variation with time, where the resistance first rapidly increased and subsequently reached stable value within a short time. The steady-state resistance R increased with the increment of the heating current I. We fitted the $R^{-1} - I^2$ curve shown in Figure 3b, which exhibits an ideal linear relationship (linear correlation coefficient $r = -0.99997$) and satisfactorily agrees with our theoretical deduction. Subsequently, the suspended ribbon was heated externally in the temperature-controlled chamber and we measured the $R - T$ relationship by a small current I_0 avoiding Joule heating effect (the entire inside of the small chamber was heated to a series of steady temperatures for a long time by the external heat equipment, and we measured the corresponding steady resistances of the suspended sample). It exhibits a linear $R - T$ relationship ($r = 0.99992$) when the temperature of the specimen varies in the small range, as shown in Figure 3c.

As a consequence, we can calculate the apparent thermal conductivity $\kappa_{\text{ap}} = 567 \pm 29$ W m^{-1} K^{-1} based on the previous theoretical analysis, it is obviously greater than the previously reported values for the randomly oriented SWNT films (23–83 W m^{-1} K^{-1})[19,26] and aligned CNT films (200–472 W m^{-1} K^{-1}).[17,26] The enormous deviation results from neglecting the radiant heat loss. It should be emphasized that, the optical photograph (Figure 2a) and large magnification scanning electron microscope (SEM) image (Figure 2b) indicate a small amount of pore exists in these SWNT thin films. We cannot obtain the κ by calculating g_{rad} because A_{rad} is unknown. However, according to our theoretical analysis, we can in situ change the L (12, 10, 8, and 6 mm) of the same specimen in our specific stage and then measure corresponding κ_{ap} (338 ± 19, 258 ± 18, 176 ± 16, and 124 ± 10 W m^{-1} K^{-1}) for fitting $\kappa_{\text{ap}} - L^2$ curve (Figure 3d), which shows the κ_{ap} varies linearly with L^2. We can obtain the thermal conductivity $\kappa = 51 \pm 5$ W m^{-1} K^{-1} by the intercept of $\kappa_{\text{ap}} - L^2$ curve, which is satisfactorily consistent with the previously reported values.[19,26] The value is about two orders of magnitude below the intrinsic thermal conductivity of individual SWNT due to the huge thermal resistance of inter-tube junctions in the SWNT networks.[19] The measurement of through-plane thermal conductivity for the thin CNT films (hundreds of nm in thickness) requires specific techniques that are not available to us currently. Based on previous report,[8] and the microstructures of our CNT films, the through-plane conductivity should be quite small. The CNTs in our films are primarily aligned in-plane, so the through-plane thermal conductivity is greatly hampered by the ubiquitous inter-tube junctions. Further discussions about thermal conductivity measurement are in the Supporting Information for experimental details.

The Seebeck coefficient and electrical conductivity measurements of the same suspended specimen can also be performed with the steady method and the standard four-electrode method, respectively, in the specific testing stage (see the Supporting Information for experimental details). We measured the σ and S in the chamber at the atmosphere. Figure 3e,f shows the V–I curve and $\Delta V - \Delta T$ curve, respectively. We obtain the $\sigma = 3.21 \times 10^5$ S m^{-1} and the apparent Seebeck coefficient $S_{\text{ap}} = 86.01$ μV K^{-1}. Taking account of the Seebeck coefficient of the copper leads $S_{\text{leads}} = 1.95$ μV K^{-1},

DOI: 10.1002/smll.201600501

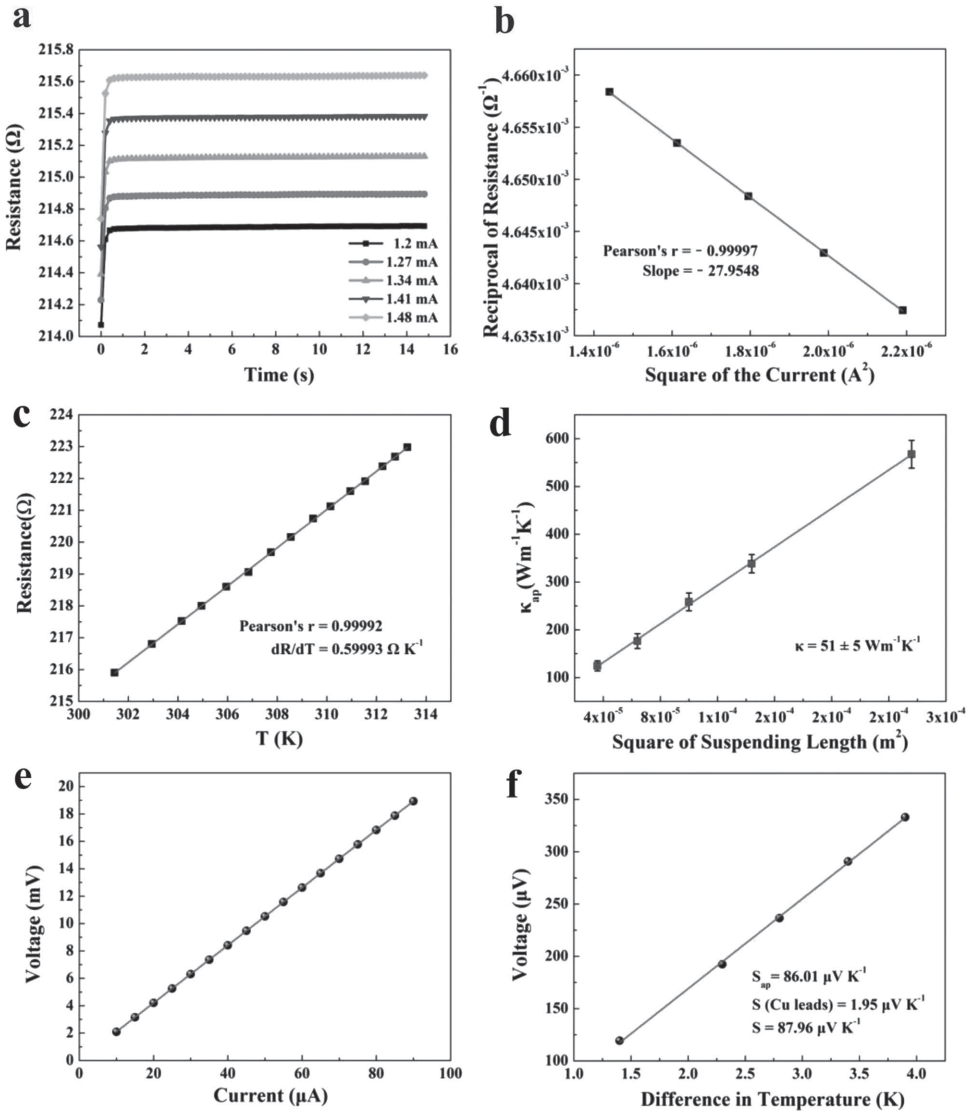

Figure 3. Thermoelectric properties of a SWNT film with 316 nm in thickness. The in-plane thermal conductivity measurement in a stabilized vacuum of 6×10^{-4} Pa: a) The resistance of the suspended ribbon variation with time under different heating current. b) The obtained R^{-1}– I^2 curve. c) The measured R–T curve in a small temperature range. d) The square of the suspended length dependence of the apparent thermal conductivity. The Seebeck coefficient and electrical conductivity measurements in the atmosphere: e) The measured V–I curve within a small range of current (10–90 μA). f) The measured steady voltage difference in different steady temperature difference between two ends of the suspended ribbon.

the S of the suspended SWNT ribbon is 87.96 μV K^{-1}. The positive Seebeck coefficient in SWNT films results from oxygen doping in air, which is suggestive of hole-like carrier.[27,28]

As a result, we can calculate the power factor PF = 2482 μW m^{-1} K^{-2} at room temperature, which is among the highest value ever reported for flexible CNT-based or organic TE materials,[8–12,14,20–22] approximately half of Bi_2Te_3 (PF = 5062 μW m^{-1} K^{-2} at T = 320 K).[23] However the density of Bi_2Te_3 ($\rho \approx 7.9$ g cm^{-3}),[1] is much larger than that of our SWNT films ($\rho \approx 1.1$ g cm^{-3}, which was obtained by measuring the mass of a densified rectangle piece through ultra-micro balance. For example, the mass of a 16 mm × 11 mm piece cut from SWNT film with a densified thickness of 316 nm is 58.9 μg, from which a density of 1.06 g cm^{-3} can be calculated), which indicates our SWNT films possibly have larger power densities. For comparison, power factors of flexible TE materials in recent researches and our works are listed in Figure 5f.

The ultrahigh power factor can be attributed to the prominent electrical conductivity and a reasonably high Seebeck coefficient of the as-grown SWNT films. It has been well-known that the electrical conductivity of the films is dominated by the inter-tube junctions. For the conventional CNT buckypaper, the contacts of inter-tube junctions formed near room temperature are weak and blocked by some highly insulating surfactant residues, which significantly degrade the electrical conductivity.[29] Additionally ultrasonic dispersing process will make CNT shorten or introduce some defects, which also further reduce σ. For example, Zhao et al. fabricated carbon nanotube papers (thickness ≈ 50 μm) through drying dispersed CNT solutions in an oven, which exhibit a low electrical conductivity of 4.8×10^3 S m^{-1} and Seebeck coefficient of 50 μV K^{-1}.[8] Recently, the SWNT

DOI: 10.1002/smll.201600501

film (thickness is in the range of 50–130 μm) prepared from semiconducting SWNT solutions shows a high Seebeck coefficient of 170 μV K^{-1} but low electrical conductivity of 1.7×10^3 S m^{-1}. To improve the conductivity, the films were treated with HNO_3. Although the σ was dramatically increased to 1×10^5 S m^{-1}, the S is decreased to 20 μV K^{-1} because of the strong p-type doping effect.[10] Thick CNT films can also be obtained from CNT forests.[16,17] The as-prepared aligned CNT buckypaper possesses a high electrical conductivity of 6.4×10^4 S m^{-1} and thermal conductivity of 500–700 W m^{-1} K^{-1}.[16] The superior thermal conductivity is not suitable in thermoelectric applications.

Whereas in our as-grown SWNT films, the bundles firmly connect with each other leading to perfect and long inter-bundle connections and form a continuous conductive network when they are growing at high temperature avoiding ultrasonic dispersing process and the use of surfactant, which result in superior structure (RAMAN spectra are shown in Figures S4 and S5, Supporting Information) and outstanding electrical conductivity.[25] We measured the thermoelectric properties of purified SWNT buckypaper (thickness ≈ 30 μm) and as-grown SWNT film for comparison, which are shown in Figure S6 (Supporting Information).

Thermoelectric properties of various SWNT films were measured and we denoted them as SWNT film 1–3, which have thicknesses of 316 ± 14, 340 ± 20, and 656 ± 20 nm, respectively. All of them exhibit prominent electrical conductivities of 3.21×10^5, 4.74×10^5, and 3.57×10^5 S m^{-1}, respectively (**Figure 4**b). SWNT film 2 has a higher σ, which is probably due to a higher content of metallic SWNTs in film 2. The Seebeck coefficient measurements indicate SWNT film 2 has an obvious lower S (59.1 μV K^{-1}) compared with film 1 and 3 (80–90 μV K^{-1}) agreeing with our assumption, which is consistent with the recent research of Maniwa and co-workers.[10] In their work, various SWNT films with different metallic–semiconducting ratios were prepared, where a controlled semiconducting ratio (α) were obtained through density gradient ultracentrifugation. Systematic measurements suggested that S monotonically increased with increasing α, nevertheless the variety of σ had an opposite trend. The UV–vis–NIR absorption spectra can further qualitatively verify our assumption, as shown in Figure 4d. The films having larger Seebeck coefficient exhibit more significant absorption peaks S_{11} and S_{22} in the range of 0.5–1.5 eV, which correspond to electron transitions between van hove singularities in semiconducting SWNTs, where the absorption peaks near 4.5 eV is attributed to π electron plasmon.

The thermal conductivities of SWNT film 1–3 are in the range of 43 ± 4 to 51 ± 5 W m^{-1} K^{-1} (Figure 4a). For comparison, we also measured a CNT sheet having a similar thickness (629 ± 17 nm), which is prepared by superposing multilayer continuously producing CNT films (the single layer thickness is ≈20 nm) and densified by ethanol. It is almost opaque (Figure 2c), which has relatively lower $\sigma = 1.37 \times 10^5$ S m^{-1} and $\kappa = 21 \pm 2$ W m^{-1} K^{-1} compared to the as-grown SWNT films. It could be understood by assuming that the contacts of inter-tube or inter-bundle junctions between the single layer CNT films are relatively weak. The additionally introduced interfacial electrical and thermal resistances slightly decrease the electrical and

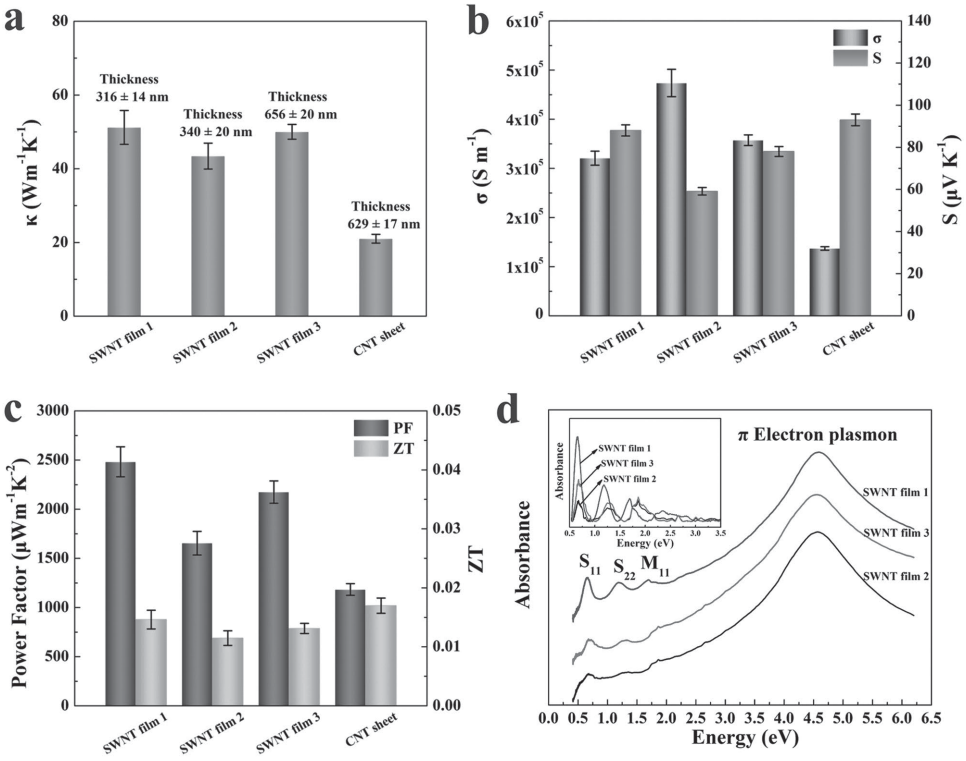

Figure 4. Thermoelectric properties of various SWNT films at room temperature. a) The measured in-plane thermal conductivities. b) The measured electrical conductivities and Seebeck coefficients. c) The calculated thermoelectric power factors and ZT values. d) The UV–vis–NIR absorption spectra of different SWNT films. The inset shows the normalized absorption spectra removed absorbing background of π electron plasmon.

DOI: 10.1002/smll.201600501

thermal conductivity. When the thickness of CNT sheet is much larger (≈15 μm), the thermoelectric properties are similar but the sheet resistance is lower (≈0.5 Ω, see Table S3, Supporting Information), which is in favor of fabricating a practical TE module with a low internal resistance.

The power factor and ZT are calculated based on the measurement results of thermoelectric properties, as shown in Figure 4c. The as-grown SWNT films exhibit excellent power factors of 1654–2482 μW m^{-1} K^{-2} at room temperature. Although the σ of film 2 is much higher, the relative low *S* results in a slightly decreased power factor of 1654 μW m^{-1} K^{-2} compared to the film 1 and 3. Estimated ZT of 0.74–1.86 were obtained based on a typical reported value for the out-of-plane thermal conductivity of 0.4–1 W m^{-1} K^{-1}.[8] Accurate ZT (maximum ≈ 0.02 at room temperature) can be obtained by measurement results of the in-plane thermal conductivity, which is higher than typical values of bulk semiconductor materials such as silicon (ZT ≈ 0.01).[30]

CNT and their composite fibers can be used to prepared wearable and functional fabrics.[31,32] The SWNT fibers obtained by twisting the as-grown SWNT films with excellent thermoelectric power factor are ideal electronic yarns, which enable us to obtain the novel and efficient thermoelectric fabrics for specific applications, e.g., harvesting biothermal energy to supply low-power biological and medical sensors. We have also researched the thermoelectric properties of the SWNT fibers. 40 mm × 5 mm ribbons were cut from the same SWNT film for twisting the SWNT fibers. The SWNT fibers 1–3 were obtained by directly twisting the pristine SWNT ribbons. On the other hand, the SWNT fiber 4 was obtained

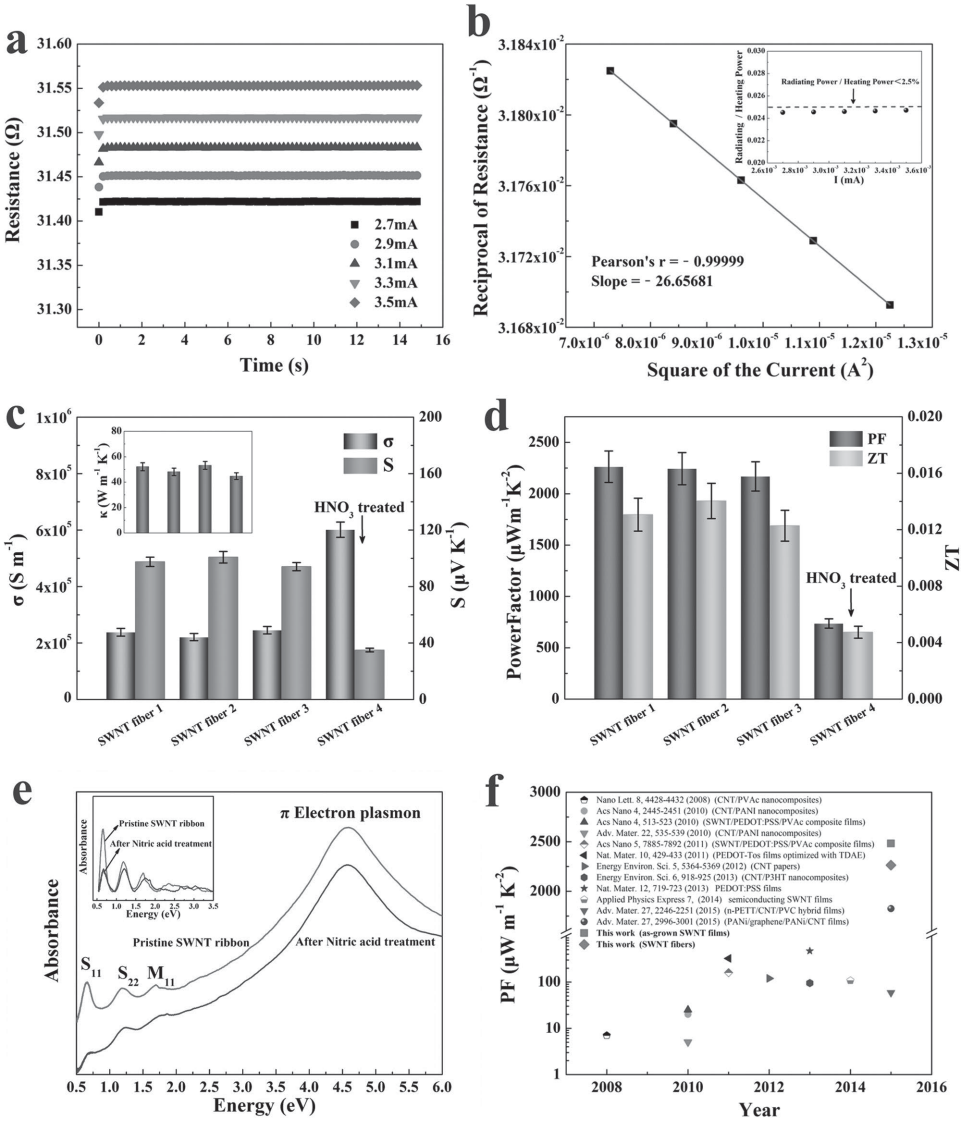

Figure 5. Thermoelectric properties of various SWNT fibers at room temperature. The thermal conductivity measurement of the SWNT fiber 1 with a diameter of 29 μm in a stabilized vacuum of 6×10^{-4} Pa: a) The resistance of the suspended fiber variation with time. b) The obtained $R^{-1} - I^2$ curve. The inset shows the ratios of radiant power to heating power. c) The measured electrical conductivities, thermal conductivities, and Seebeck coefficients of the SWNT fibers 1–4. d) The calculated thermoelectric power factors and ZT values of the SWNT fibers 1–4. e) The UV–vis absorption spectra of a SWNT ribbon before and after nitric acid immersing. The inset shows the normalized absorption spectra removed absorbing background of π electron plasmon. f) Power factors of flexible TE materials in recent researches and our works.

DOI: 10.1002/smll.201600501

by twisting the treated SWNT ribbon, which was immersed in 10 M Nitric acid for 5 h and subsequently washed with deionized water repeatedly. Figure 2d shows the SEM photograph of the SWNT fiber 1 with a diameter of 29 μm. **Figures 5**a,b shows the resistance variation with time and $R^{-1} - I^2$ curve during the thermal conductivity measurement, which likewise satisfactorily agree with our theoretical deduction. For the fiber with a short suspended length, the radiant heat loss can be neglected resulting in thermal conductivity $\kappa \approx \kappa_{ap} = 53$ W m^{-1} K^{-1} because the ratios of radiant power to heating power are less than 2.5% under all the heating currents (inset of Figure 5b).

The SWNT fibers 1–3 exhibit similar thermoelectric performances (Figure 5c). The calculated power factors are as high as 2169–2263 μW m^{-1} K^{-2}. Nitric acid treatment is a conventional and effective purified method for the CNT films assembled with vacuum filtration or spraying. After the nitric acid treatment, the intrinsically poor electrical conductivity has an enormous improvement attributed to both removal of insulating dispersing agents and strong p-type doping effect.[29,33] The influence of nitric acid treatment on our SWNT specimens is revealed by comparing the thermoelectric performance of SWNT fibers 1–3 and 4. The fiber 4 twisted from the treated ribbon has a dramatically higher σ (6.01×10^5 S m^{-1}) compared to the SWNT fibers 1–3 ($\sigma \approx 2.3 \times 10^5$ S m^{-1}). In contrast, the SWNT fiber 4 shows a distinctly lower S (35 μV K^{-1}) compared to the SWNT fibers 1–3 ($S \approx 100$ μV K^{-1}), which is suggestive of a stronger hole-doping process resulting from the nitric acid treatment. Furthermore, the UV–vis–NIR absorption spectra shown in Figure 5e for a SWNT ribbon before and after nitric acid immersing clearly show strong doping-induced attenuation of the S_{11} and S_{22} transitions, which is in agreement with previous reports.[33–35]

In summary, the pristine as-grown SWNT interconnected films have prominent structure and electrical conductivities so that conventional nitric acid treatment can be omitted, which avoid strong p-type doping effect[33–35] and make our SWNT films retain relatively high Seebeck coefficient. As a result, our as-grown SWNT films and fibers exhibit ultrahigh thermoelectric power factors ($PF_{max} = 2482$ μW m^{-1} K^{-2} at room temperature), which is among the highest value ever reported for flexible CNT-based or organic TE materials.[8–12,14,20–22] In addition, these SWNT-based materials avoid tedious composite technology. The TE module composed of several p–n couples can be utilized for directly converting heat into electric energy without moving mechanical components or hazardous working fluids.[36] The as-grown SWNT films can be switched into n-type films by functionalization with electron-rich polymers or small molecules,[37,38] which will enable us to fabricate a high-performance and flexible TE module.

What's more, we introduced an ingenious strategy for accurately and efficiently evaluating thermoelectric performance of micro-nano films and fibers. Based on our measuring method and apparatus, we can efficiently measure thermoelectric properties (S, σ, κ) for the same film in the in-plane direction and the same fiber in the axial direction. For the measurement of thermal conductivity, the specimen itself serves both as a heater and a temperature sensor, obviating the need of external heating source and thermometers. This is a great advantage over previous methods, especially for thin and porous films, the heat losses through convection and radiation have been eliminated during the measurement.

Estimated ZT of 0.74–1.86 is obtained if a typical reported value for the out-of-plane thermal conductivity of 0.4–1 W m^{-1} K^{-1} is cited.[8] In contrast, our measurement results of the in-plane thermal conductivity are satisfactorily consistent with the previously reported values, which result in accurate evaluations of ZT (maximum ≈ 0.02 at room temperature). Compared to the conventional inorganic TE materials, the as-prepared SWNT films and fibers with remarkable power factors and unique advantages have enormous competitiveness in portable thermoelectric conversion and novel sensing applications.[39]

Supporting Information

Supporting Information is available from the Wiley Online Library or from the author.

Acknowledgements

This work was supported by the National Basic Research Program of China (Grant No. 2012CB932302), the National Natural Science Foundation of China (51172271, 51372269, and 51472264), and the "Strategic Priority Research Program" of the Chinese Academy of Sciences (XDA09040202). Dr. H. P. Liu thanks support by the Recruitment Program of Global Youth Experts and the "100 talents project" of CAS.

[1] C. Yu, Y. S. Kim, D. Kim, J. C. Grunlan, *Nano Lett.* **2008**, *8*, 4428.
[2] R. S. Prasher, X. J. Hu, Y. Chalopin, N. Mingo, K. Lofgreen, S. Volz, F. Cleri, P. Keblinski, *Phys. Rev. Lett.* **2009**, *102*, 105901.
[3] D. Kim, Y. Kim, K. Choi, J. C. Grunlan, C. H. Yu, *ACS Nano* **2010**, *4*, 513.
[4] C. Z. Meng, C. H. Liu, S. S. Fan, *Adv. Mater.* **2010**, *22*, 535.
[5] Q. Yao, L. D. Chen, W. Q. Zhang, S. C. Liufu, X. H. Chen, *ACS Nano* **2010**, *4*, 2445.
[6] C. Yu, K. Choi, L. Yin, J. C. Grunlan, *ACS Nano* **2011**, *5*, 7885.
[7] C. A. Hewitt, A. B. Kaiser, S. Roth, M. Craps, R. Czerw, D. L. Carroll, *Nano Lett.* **2012**, *12*, 1307.
[8] W. Y. Zhao, S. F. Fan, N. Xiao, D. Y. Liu, Y. Y. Tay, C. Yu, D. H. Sim, H. H. Hng, Q. C. Zhang, F. Boey, J. Ma, X. B. Zhao, H. Zhang, Q. Y. Yan, *Energy Environ. Sci.* **2012**, *5*, 5364.
[9] C. Bounioux, P. Diaz-Chao, M. Campoy-Quiles, M. S. Martin-Gonzalez, A. R. Goni, R. Yerushalmi-Rozene, C. Muller, *Energy Environ. Sci.* **2013**, *6*, 918.
[10] Y. Nakai, K. Honda, K. Yanagi, H. Kataura, T. Kato, T. Yamamoto, Y. Maniwa, *Appl. Phys. Express* **2014**, *7*, 025103.
[11] N. Toshima, K. Oshima, H. Anno, T. Nishinaka, S. Ichikawa, A. Iwata, Y. Shiraishi, *Adv. Mater.* **2015**, *27*, 2246.

[12] C. Cho, B. Stevens, J. H. Hsu, R. Bureau, D. A. Hagen, O. Regev, C. Yu, J. C. Grunlan, *Adv. Mater.* **2015**, *27*, 2996.
[13] K. Kurabayashi, *Int. J. Thermophys.* **2001**, *22*, 277.
[14] O. Bubnova, Z. U. Khan, A. Malti, S. Braun, M. Fahlman, M. Berggren, X. Crispin, *Nat. Mater.* **2011**, *10*, 429.
[15] T. Borca-Tasciuc, A. R. Kumar, G. Chen, *Rev. Sci. Instrum.* **2001**, *72*, 2139.
[16] L. Zhang, G. Zhang, C. H. Liu, S. S. Fan, *Nano Lett.* **2012**, *12*, 4848.
[17] D. Wang, P. C. Song, C. H. Liu, W. Wu, S. S. Fan, *Nanotechnology* **2008**, *19*, 075609.
[18] G. Zhang, C. H. Liu, S. S. Fan, *Sci. Rep.* **2013**, *3*, 2549.
[19] M. E. Itkis, F. Borondics, A. P. Yu, R. C. Haddon, *Nano Lett.* **2007**, *7*, 900.
[20] Y. M. Sun, P. Sheng, C. A. Di, F. Jiao, W. Xu, D. Qiu, D. B. Zhu, *Adv. Mater.* **2012**, *24*, 932.
[21] G. H. Kim, L. Shao, K. Zhang, K. P. Pipe, *Nat. Mater.* **2013**, *12*, 719.
[22] T. Park, C. Park, B. Kim, H. Shin, E. Kim, *Energy Environ. Sci.* **2013**, *6*, 788.
[23] T. M. Tritt, *Annu. Rev. Mater. Res.* **2011**, *41*, 433.
[24] L. Song, L. Ci, L. Lv, Z. P. Zhou, X. Q. Yan, D. F. Liu, H. J. Yuan, Y. Gao, J. X. Wang, L. F. Liu, X. W. Zhao, Z. X. Zhang, X. Y. Dou, W. Y. Zhou, G. Wang, C. Y. Wang, S. S. Xie, *Adv. Mater.* **2004**, *16*, 1529.
[25] W. J. Ma, L. Song, R. Yang, T. H. Zhang, Y. C. Zhao, L. F. Sun, Y. Ren, D. F. Liu, L. F. Liu, J. Shen, Z. X. Zhang, Y. J. Xiang, W. Y. Zhou, S. S. Xie, *Nano Lett.* **2007**, *7*, 2307.
[26] J. Hone, M. C. Llaguno, N. M. Nemes, A. T. Johnson, J. E. Fischer, D. A. Walters, M. J. Casavant, J. Schmidt, R. E. Smalley, *Appl. Phys. Lett.* **2000**, *77*, 666.
[27] K. Bradley, S. H. Jhi, P. G. Collins, J. Hone, M. L. Cohen, S. G. Louie, A. Zettl, *Phys. Rev. Lett.* **2000**, *85*, 4361.
[28] P. G. Collins, K. Bradley, M. Ishigami, A. Zettl, *Science* **2000**, *287*, 1801.
[29] H.-Z. Geng, K. K. Kim, K. P. So, Y. S. Lee, Y. Chang, Y. H. Lee, *J. Am. Chem. Soc.* **2007**, *129*, 7758.
[30] L. Weber, E. Gmelin, *Appl. Phys. A* **1991**, *53*, 136.
[31] B. S. Shim, W. Chen, C. Doty, C. L. Xu, N. A. Kotov, *Nano Lett.* **2008**, *8*, 4151.
[32] Q. Wang, Q. Yao, J. Chang, L. D. Chen, *J. Mater. Chem.* **2012**, *22*, 17612.
[33] R. C. Tenent, T. M. Barnes, J. D. Bergeson, A. J. Ferguson, B. To, L. M. Gedvilas, M. J. Heben, J. L. Blackburn, *Adv. Mater.* **2009**, *21*, 3210.
[34] J. L. Blackburn, T. M. Barnes, M. C. Beard, Y. H. Kim, R. C. Tenent, T. J. McDonald, B. To, T. J. Coutts, M. J. Heben, *ACS Nano* **2008**, *2*, 1266.
[35] W. Zhou, J. Vavro, N. M. Nemes, J. E. Fischer, F. Borondics, K. Kamaras, D. B. Tanner, *Phys. Rev. B* **2005**, *71*, 205423.
[36] L. E. Bell, *Science* **2008**, *321*, 1457.
[37] Y. Nonoguchi, K. Ohashi, R. Kanazawa, K. Ashiba, K. Hata, T. Nakagawa, C. Adachi, T. Tanase, T. Kawai, *Sci. Rep.* **2013**, *3*, 3344.
[38] C. H. Yu, A. Murali, K. W. Choi, Y. Ryu, *Energy Environ. Sci.* **2012**, *5*, 9481.
[39] F. J. Zhang, Y. P. Zang, D. Z. Huang, C. A. Di, D. B. Zhu, *Nat. Commun.* **2015**, *6*, 8356.

Received: February 16, 2016
Revised: April 19, 2016
Published online:

DOI: 10.1002/smll.201600501